JOURNAL OF MATERIALS SCIENCE 35 (2000) 3169–3179

Review
A P/M approach for the fabrication of an orthorhombic titanium aluminide for MMC applications

P. R. SMITH, A. H. ROSENBERGER
Air Force Research Laboratory, Materials and Manufacturing Directorate, Wright-Patterson AFB, OH 45433-7817, USA

M. J. SHEPARD
Southwestern Ohio Council for Higher Education (SOCHE), Dayton, OH 45420-4014, USA
E-mail: michael.shepard@afrl.af.mil

R. WHEELER IV
Universal Energy Systems, Inc., Dayton, OH 45432, USA

A study has been undertaken to examine the feasibility of using a powder metallurgy (P/M) approach for the fabrication of an orthorhombic (O; Ti_2AlNb)-based titanium aluminide alloy intended for use as a matrix in a continuous fiber reinforced titanium matrix composite (TMC). Spherical powder of Ti-22Al-26Nb (at%) was produced using inert gas atomization. The atomized powder was sieved to -80 mesh (<177 μm) size fraction and used in the fabrication of unreinforced "neat" panels via the tape casting process. Microstructural and phase chemistry examinations of the as-produced powder, thermally exposed powder and neat matrix were conducted using back-scatter electron scanning electron microscope (BSE SEM) imaging, wavelength dispersive spectroscopy (WDS), and TEM analysis. Mechanical behavior studies of the as-fabricated and heat treated neat material included: tensile, creep and isothermal fatigue. Results obtained for the P/M-based neat material were compared to previously obtained foil-based neat data, and to those property requirements necessary to be considered for use as a matrix in the fabrication of O TMCs.

1. Introduction

Titanium aluminide alloys based upon the orthorhombic (O) phase (Ti_2AlNb) have gained significant visibility as candidate matrices for continuously reinforced metal matrix composites over the last several years [1–5]. These "O" alloys have demonstrated several key performance advantages when compared to their α_2 (Ti_3Al) predecessors, including improved ambient and elevated temperature strength, improved creep resistance, greater ambient temperature fracture toughness and reduced chemical reactivity with silicon carbide reinforcements [6]. These advantages have led orthorhombic titanium composites (O TMCs) to be considered as enabling materials for next generation gas turbine engines which require significantly improved thrust-to-weight ratios and reduced specific fuel consumption. Indeed, rotating engine hardware is currently being manufactured for demonstration which incorporate O TMCs in the compressor to take advantage of the aforementioned performance enhancements. Several major challenges remain however, before O TMCs can be successfully incorporated for military or commercial applications. Among these challenges is the need for improved affordability.

The costly production of orthorhombic alloys in foil form using conventional multi-step ingot reduction practices precludes the fabrication of affordable O TMCs. Currently, this processing route which includes forging, repeated hot rolling and cold rolling with intermediate stress relief anneals, results in the cost of orthorhombic foil being on the order of $\geq$\$700/lb. Of course this assumes that the "O" alloy is cold rollable to foil. Indeed, recent attempts to cold roll orthorhombic alloys which contained higher order additions such as Mo and Si to foil on a production mill were unsuccessful [7].

The subject study begins to address the issue of composite affordability by assessing the viability of a low-cost powder-based (powder cost $\leq$\$70/lb.) composite fabrication approach, tape casting, to produce an orthorhombic ternary alloy with adequate mechanical performance, so as to be considered for use as a matrix for O TMCs.

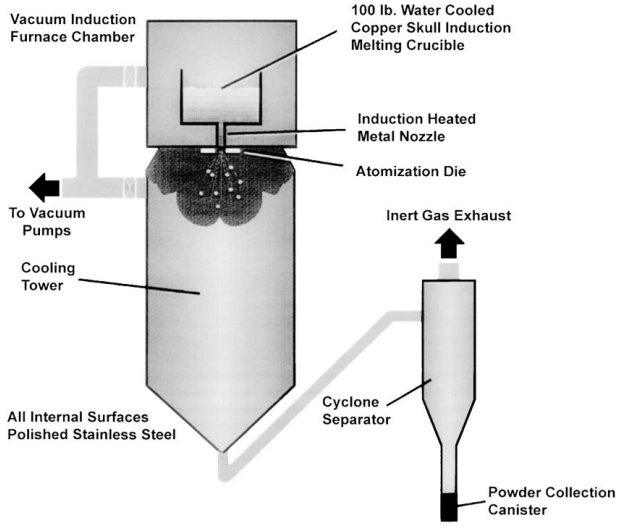

Figure 1 Schematic figure of gas atomization process used to produce powders.

2. Experimental procedure

The "O" composition Ti-22Al-26Nb (at%) was selected for the subject study based upon previous results by Rowe [8], wherein he demonstrated that this alloy exhibited the best balance of mechanical properties from a series of ternary compositions examined in monolithic form. The alloy was produced as spherical powder by Crucible Research Center using inert gas atomization. A schematic of Crucible's gas atomization process is shown in Fig. 1. The nominal Ti-22Al-26Nb composition was formulated by the use of master alloys and elemental additions which were melted in a water-cooled copper crucible. During melting, the alloy formed a protective titanium skull that prevented the copper tundish from reacting with the molten metal. The liquid metal was poured through an induction-heated nozzle and subsequently through a die, where upon exit, the molten stream was impinged with argon gas which acted to atomize the metal into spherical droplets that were rapidly solidified. The resultant powder was collected and sent to a cyclone separator. Additional details regarding Crucible's gas atomization process can be found elsewhere [9].

The Ti-22Al-26Nb powder was screened to -80 mesh (<177 μm), to enable Atlantic Research Corporation (ARC) to fabricate flat neat (unreinforced) panels (150 mm $\times$ 230 mm $\times$ 0.5 mm) via tape casting and hot isostatic pressing (HIP'ing). -80 mesh powder is required for composite fabrication so that the powder can fit between the fibers. In the tape casting process, Ti-22Al-26Nb powders were mixed with an organic binder and spread to form a green tape. Multiple tapes were stacked on top of one another and diffusion-bonded via HIP'ing to form a neat panel. More detailed information regarding the tape casting process is available elsewhere [10]. The HIP'ing profile (time/temperature/pressure) used to consolidate the tapes into neat matrix material is shown in Fig. 2. It was selected such that the maximum temperature excursion remained below the beta solvus of the ternary alloy in an attempt to prevent excessive grain growth.

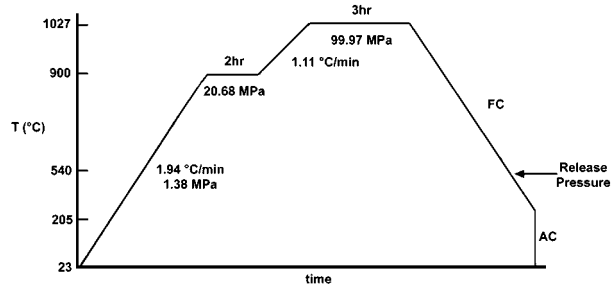

Figure 2 Time/Temperature/Pressure profile used in the HIP consolidation of the "neat" panels.

Samples of as-produced powders and as-fabricated neat material were analyzed for bulk composition of major alloying elements, as well as, for interstitial content using standard wet chemistry and x-ray florescence techniques. Back-scatter electron (BSE) imaging in the scanning electron microscope (SEM) was conducted on as-atomized powder surfaces, cross-sectioned powders and consolidated neat material to elucidate microstructural details. In addition, loose powders were subjected to the thermal cycle used to consolidate the neat material, and subsequently examined by BSE microscopy in an attempt to simulate microstructural evolution during the consolidation process. Local composition was obtained using wavelength dispersive spectroscopy (WDS) on polished cross-sections of powder and consolidated neat specimens. A total of ten WDS samplings were collected for each condition. TEM analysis of neat material was carried out on a Philips CM200 FEG microscope. The small probe characteristics of this instrument allow both fine and coarse microstructural features to be imaged and local phase compositions to be determined. The microstructures evaluated by TEM were related to those obtained via SEM.

A beta solvus approach curve was obtained for Ti-22Al-26Nb using the disappearing phase technique, wherein samples were solution heat treated for 2 hours at systematically increasing temperatures (25°C increments) followed by oil quenching. In addition, attempts to validate the solvus temperature was made using differential thermal analyses (DTA). Endothermic and exothermic inflection points were taken from the DTA heating (35°C/min.) and cooling (35°C/min.) curves, respectively, to assess phase boundary temperatures.

Previous studies on neat foil-based Ti-22Al-23Nb had indicated that improved levels of mechanical performance could be obtained via post-consolidation solutionizing and aging heat treatments [11]. These improvements were observed to be related to the constituency of equiaxed primary α_2 and lenticular "O" phases. In particular, as the volume fraction of primary α_2 decreased, and correspondingly, the volume fraction of the lenticular "O" phase increased, gains in tensile and creep performance were observed. In a parallel study, Graves [12] found reduced levels of room temperature ductility in powder metallurgy produced neat Ti-22Al-23Nb, which he attributed to the formation of a continuous network of primary α_2. Therefore, in the subject study, a series of heat treatments were developed using the beta solvus approach curve obtained for the

Ti-22Al-26Nb composition, with the intent of dissolving the primary α_2 phase, while producing increased levels of the lenticular "O" phase.

Dogbone specimens measuring 101 mm (l) × 10 mm (w) with a reduced gage section width of 6 mm formed by a 40 mm radius were cut from neat panels using electron discharge machining (EDM). The recast layers formed at the specimen edges during EDM were removed by diamond polishing. All testing was performed in a laboratory air environment on a horizontal computer controlled servo-hydraulic MTS system using test software described by Hartman and Russ [13]. Loading was accomplished through the use of precision-aligned hydraulic friction grips, while strain was monitored by high temperature, quartz rod extensometry. A 25 mm portion of the gage section was uniformly heated for elevated temperature testing, while the specimen tabs where kept nearly at room temperature through the use of water-cooled grips. Heating was accomplished via a series of quartz lamps oriented perpendicular to the specimen, while temperature was measured and controlled through the use of four thermocouples that were welded to the specimen surface, providing for four zones of control with two lamps per zone. Stroke-controlled tensile tests were conducted over the temperature interval of 23–760°C at a constant crosshead speed of 0.012 mm/s, resulting in a strain rate of $\sim 10^{-4}$/s. Test conditions (stress/temperature) for elevated temperature creep studies were selected to enable rupture lives not to exceed 300 hours. During creep testing, the specimens were first heated to the requisite test temperature, and were then loaded at a rate of 50 MPa/s until the desired sustained load was obtained. Isothermal fatigue testing was conducted using a sinusoidal waveform at a frequency of 10 Hz, a stress ratio of $R = 0.1$, at temperatures of 23°C, 430°C and 650°C. Fractography was performed using secondary electron imaging (SEI) via SEM on selected samples to determine failure locations and mechanisms.

3. Results and discussion

3.1. Compositional and microstructural analysis

Bulk compositional analysis for the Ti-22Al-26Nb alloy in −80 mesh (<177 μm) as-produced powder and as-consolidated neat matrix forms are shown in Table I. The measured levels for the main alloying elements (Al, Nb) were found to be very close to the desired nominal values. However, there was one noteworthy trend observed for the interstitial results for O and C. The O and C levels were seen to increase when going from loose powder to neat matrix form. This result may be due to two factors: 1) small amounts of organic binder left from the tape casting process (O, C); and 2) absorption of O during subsequent HIP'ing of the panels. Regardless of the mechanism responsible for the observed increases in interstitial content, their levels likely played a role in both the microstructural development and mechanical performance of the alloys, as will be discussed later.

Fig. 3 shows a BSE image of the as-atomized powder surface. It can be noticed that a dendritic cellular network has formed upon solidification. The scale of this network was influenced by the solidification rate of the individual powders, which in turn was dependent upon the powder diameter. Rapid solidification during gas atomization from the molten state results in a metastable structure, which for a similar "O" alloy made using gas atomization, was determined to be entirely retained beta [9].

BSE images of the powder cross-sections after exposure to the neat matrix thermal consolidation cycle are displayed in Fig. 4. Considering the ternary phase diagram of Rhodes [14], compositional and contrast analyses indicated that the microstructure consisted of three phases: a dark equiaxed phase, alpha-2 (α_2; Ti_3Al; HCP/DO_{19}); a light gray lenticular phase, orthorhombic (O; Ti_2AlNb); and a white continuous phase, beta (β_0/β; BCC). The alpha-2 and orthorhombic phases have been

TABLE I Bulk compositions for powder and neat matrix, measured by wet chemical analysis

Ti22Al26Nb	Al wt% (at%)	Nb wt% (at%)	C wt% (at%)	N wt% (at%)	O wt% (at%)	H wt% (at%)
Powder	10.2(20.8)	43.6(25.8)	0.036(0.16)	0.009(0.04)	0.086(0.30)	0.003(0.14)
Neat	10.4(21.3)	44.4(26.3)	0.050(0.23)	0.006(0.02)	0.108(0.37)	0.002(0.11)

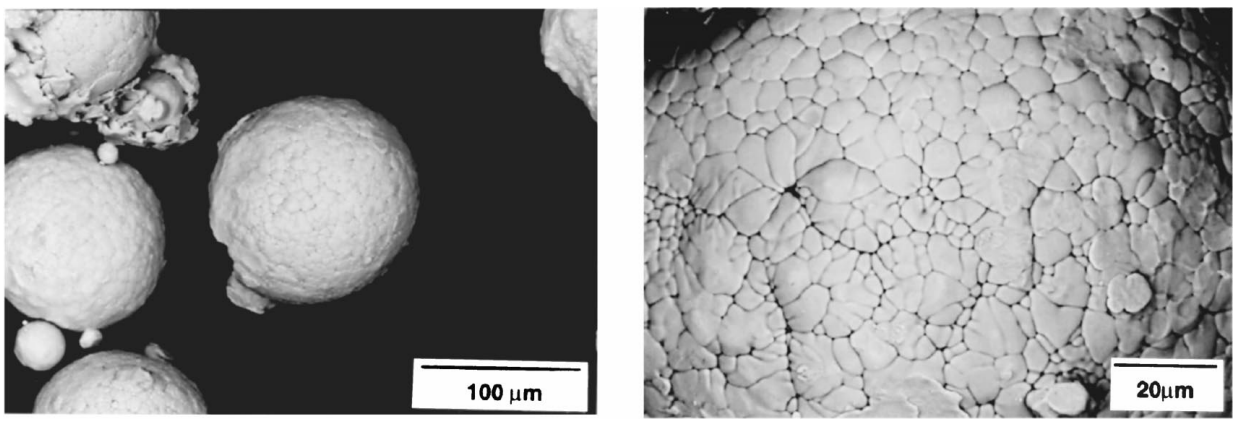

Figure 3 BSE images of the as-atomized powder surface for Ti-22Al-26Nb.

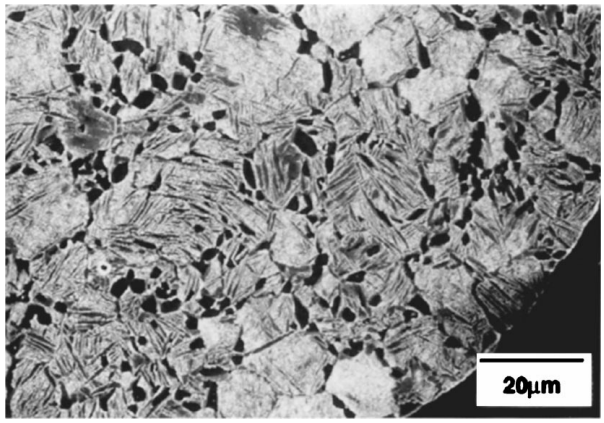

Figure 4 BSE image of the powder cross-section after exposure to the neat matrix thermal consolidation cycle.

shown to be ordered in similar alloy compositions. However, depending on the Al content of the beta phase, it has been observed to be present in both ordered (β_0) or disordered (β) forms [14]. Hence, the beta phase will be referred to as β/β_0 until results discussing TEM diffraction studies and phase composition are presented. The morphological arrangement of the phases which evolved in the thermally exposed powders seemed to correspond to the dendritic network previously observed for the as-atomized powders. This dendritic network, which formed a cellular pattern on the order of 10–20 μm, evolved into a semi-contiguous necklacing of primary equiaxed α_2 grains in the thermally exposed powder, which appeared to form at the previous cell boundaries. Conversely, the cell interiors of the as-atomized powder, evolved into a mixture of coarse lenticular "O" phase platelets surrounded by continuous beta (β/β_0) phase, for the thermally treated powder.

Fig. 5 contains BSE images of the as-consolidated neat matrix microstructure. This microstructure contained the same three phases as found in the thermally exposed powder, with an essentially analogous phase arrangement. Again, the primary α_2 formed a semi-contiguous network, while "O" platelets precipitated within the β/β_0 matrix. Thus, the origin of the as-consolidated neat matrix microstructure, like that of the thermally treated powders, could be traced to the cellular dendritic structure found in the as-atomized powders.

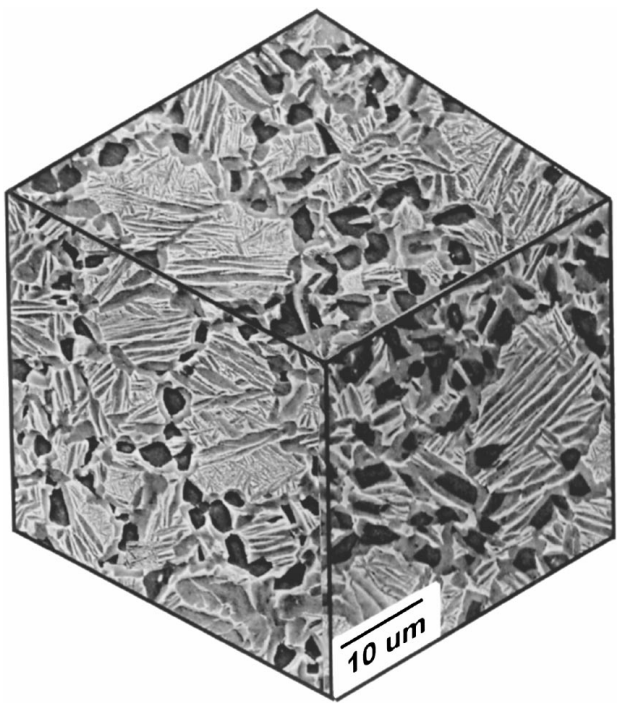

Figure 5 BSE images of the as-consolidated neat matrix microstructure for tape cast Ti-22Al-26Nb.

TABLE II Local compositions in microstructure determined by WDS microprobe analysis

Material	Location in Microstructure	Al (at%/σn)	Nb (at%/σn)
As-Atomized	Center	20.3/0.5	30.6/1.0
Powder	Boundary	24.1/0.4	21.1/1.0
Heat-Treated	$O + \beta_0/\beta$	21.4/0.2	27.3/0.2
Powder	α_2 Region	25.2/0.3	16.0/1.0
Neat Matrix	$O + \beta_0/\beta$	21.0/0.1	28.4/0.2
	α_2 Region	25.1/0.1	16.3/0.4

The explanation for the aforementioned microstructural evolution can be found by examining the local composition of the alloy. The WDS microprobe data for the three conditions discussed above (i.e. as-atomized powder, thermally exposed powder, and as-consolidated neat matrix) is shown in Table II. The data was collected from two regions for each condition. For the as-atomized powder, data was taken from both the centers of the cellular regions, as well as, at the cell boundaries. Data for the thermally exposed powder and the as-consolidated neat matrix conditions were taken from the α_2 and $O + \beta/\beta_0$ regions. The cell interior of the as-atomized powders was found to be rich in Nb and lean in Al. Conversely, the cell boundaries were rich in Al and lean in Nb. These observations were consistent with constitutional supercooling of the molten droplets during gas atomization. Under these conditions, the last liquid to solidify at the cell boundaries was high in Al. The interior of the cellular regions which contained high levels of Nb, tended to precipitate lenticular "O" platelets from within the β/β_0 phase upon thermal exposure. This was consistent with Nb being a stabilizer of the "O" and β/β_0 phases. Conversely, those regions high in Al tended to form the primary α_2 phase upon thermal exposure, once again consistent with Al being a particularly strong α_2 stabilizer [15]. The end result is a neat matrix microstructure previously shown in Fig. 5, which consists of a semi-contiguous network of primary α_2 and regions of "O" platelets in a β/β_0 matrix.

The "O" platelets were too fine in scale to enable the "O" and β/β_0 chemistries to be separately discerned by the microprobe. However, transmission electron microscopy (TEM) elemental analysis provided a higher spatial resolution, isolating the individual phase compositions in the neat material. Here, phase morphology, composition and degree of order were examined. A typical bright field TEM microstructure for the ternary alloy is shown in Fig. 6. Several large, interconnected α_2 grains are labeled here. Unlike similar areas imaged in the SEM, these grains were observed to exhibit

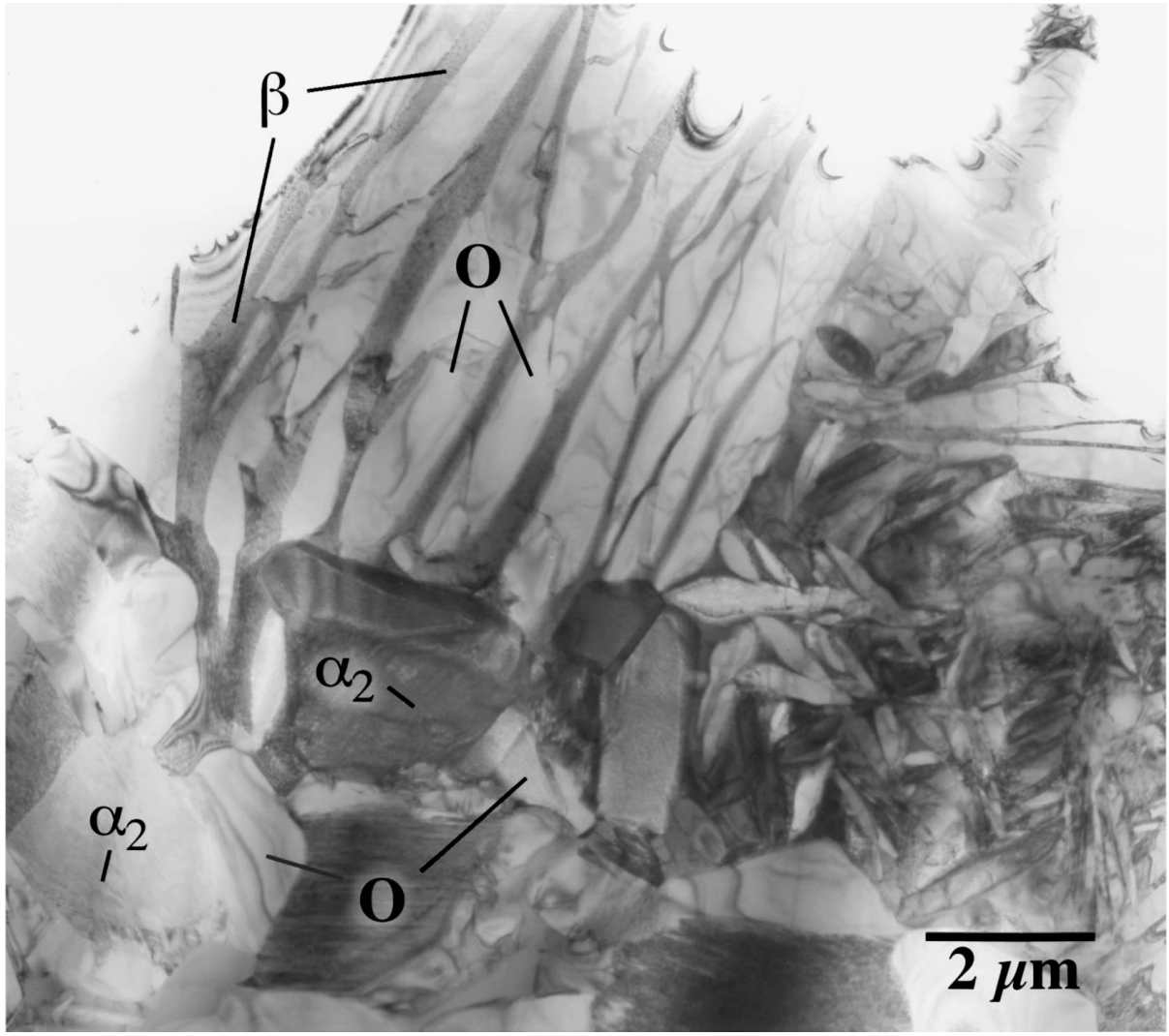

Figure 6 Bright field TEM image showing different phases present in tape cast Ti-22Al-26Nb.

extensive faulting. A region of α_2 surrounds a large domain of coarse $O + \beta/\beta_0$ which was easily identified with like areas in the SEM image in Fig. 5. A significant amount of blocky "O" phase was also present along the $O + \beta/\beta_0$ domains. The nature of order in the beta phase matrix can be determined from the selected area diffraction (SAD) pattern in Fig. 7. The [001] crystallographic orientation of the beta matrix is aligned with the electron beam direction. In this zone axis orientation, the (110), (200) and (020) reflections are present, consistent with the disordered beta structure. The absence of {100} type reflections also excludes assigning the ordered β_0 or B2 structure for this phase.

Table III displays the compositional analysis of the individual phases in the as-consolidated neat matrix condition as determined by energy dispersive x-ray spectroscopy (EDS) in the TEM. Here, a well-characterized ternary Ti-Al-Nb alloy standard was used in the quantitative EDS analysis. It can be observed that the Al content of the beta phase was on the order of 8.7 at%. Rhodes [14] had previously observed

TABLE III Compositions of phases in as-consolidated neat matrix obtained via TEM EDS analysis

Phase	Al (at%/σn)	Nb (at%/σn)
β	8.7/1.0	43.0/1.6
O	24.5/0.6	25.5/0.4
α_2	24.4/0.2	16.6/0.1

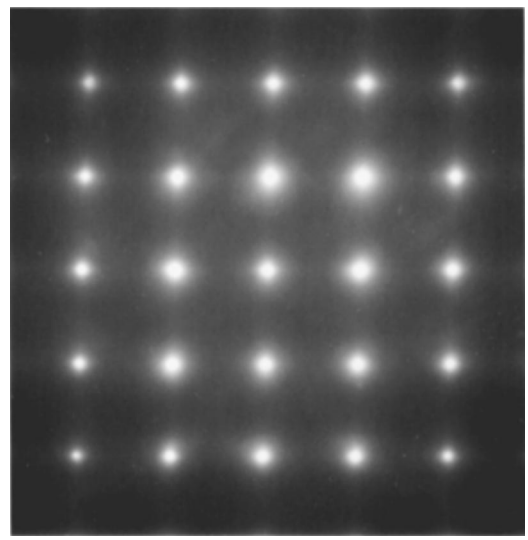

Figure 7 Selected area diffraction (SAD) pattern for as tape cast Ti-22Al-26Nb.

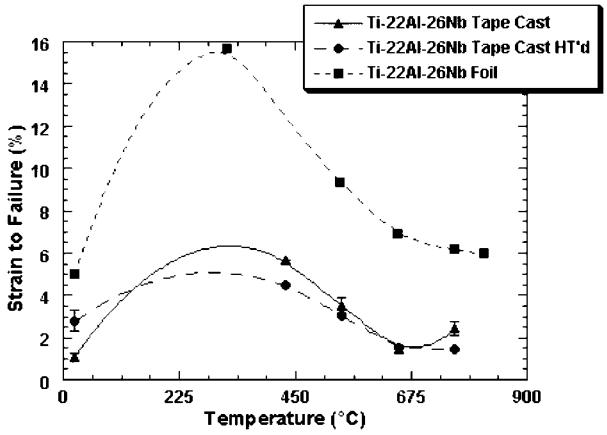

Figure 8 Strain to failure as a function of temperature for as-consolidated alloys.

for similar "O" alloys that when the Al content was $\leq \sim$12 at%, the beta phase tended to disorder, which is consistent with the SAD results. Henceforth, the beta phase in the present study will be referred to as disordered beta (β).

3.2. Mechanical properties-as fabricated

3.2.1. Tensile ductility

Fig. 8 displays the strain-to-failure for the neat Ti-22Al-26Nb in the as-fabricated condition as a function of temperature from 23–760°C. Also included for comparison is foil-based neat Ti-22Al-26Nb data from Ashbaugh [16]. Previous studies of SiC reinforced titanium alloys had indicated a minimum requirement for matrix room temperature ductility of approximately 2.5–3.0% in order obtain rule of mixtures tensile strength in the composite [17]. This minimum ductility requirement is needed to accommodate two factors: 1) the tensile residual stress in the matrix, which arises during composite fabrication due to the difference in coefficient of thermal expansion between the matrix and fiber; and 2) the elastic strain needed to load the fiber to its maximum strain capability. It can be noticed that the P/M Ti-22Al-26Nb alloy in the as-fabricated condition did not satisfy this room temperature ductility requirement, exhibiting strain-to-failure value of 1.1%. This result is in contrast to that for the Ti-22Al-26Nb foil-based composition, which exceeded the room temperature ductility requirement, averaging $\sim$5.0%. The reason for the higher ductility in the latter was most likely the result of the thermomechanical processing the foil-based composition underwent to produce 0.13 mm thick foil, which was used in the fabrication of the neat matrix. During processing to foil, the Ti-22Al-26Nb alloy undergoes significant hot and cold working, such that both microstructural and crystallographic texturing can occur [18]. It is probable that one or both forms of texturing may be responsible for the high levels of room temperature ductility observed in the foil-based alloy. Unfortunately, one limitation of the powder-based approach is the insignificant amount of hot/cold work introduced into the matrix during HIP'ing, and thus, little to no microstructural and/or crystallographic texturing of the matrix. Both the powder-based and foil-based systems showed consistent ductility behavior with temperature, such that a maximum ductility was observed at intermediate temperatures (i.e. 240–450°C), while at higher temperatures, the ductility decreased. The increase at intermediate temperatures was most likely the result of increased number of slip systems being activated for the primary α_2 phase [19]. The decrease in ductility at high temperatures was most likely due to interstitial embrittlement of the matrix. Cerchiara [18] had demonstrated that interstitial embrittlement of this nature can occur very rapidly at elevated temperature in orthorhombic-based titanium aluminides.

It is assumed that the ductility of the β phase is primarily responsible for the ductility of the three phase Ti-22Al-26Nb system at ambient temperature. This postulation is based upon the limited slip character of the α_2 and "O" phases at room temperature. As previously noted, the beta phase was found to be disordered in the Ti-22Al-26Nb powder-based alloy. Therefore, one might have expected the alloy to have exhibited reasonable levels of low temperature ductility. However, the alloy demonstrated only 1.1% strain-to-failure at room temperature. One plausible explanation for this low ductility in light of the beta phase disordering may be the high levels of Nb present in the β phase. It can be noticed in Table III that the β phase contained 43 at% Nb. This high level of Nb may have acted to solid solution strengthen the alloy to such an extent that its ductility was adversely affected.

An additional explanation for the limited ductility of the P/M system at room temperature might be attributed to the presence of the aforementioned semi-contiguous network of the primary α_2 phase. Fig. 9 contains BSE image of the Ti-22Al-26Nb fracture surface after tensile testing at room temperature. It can be seen that the fracture path was through this α_2 network. Previous studies had indicated that the α_2 phase exhibited poor ductility at or near ambient temperature [19]. This was attributed to the anisotropy of slip associated with the DO_{19} structure. Slip of $\langle a \rangle$-type dislocations was observed to occur relatively easily on the prism plane, while $\langle c + a/2 \rangle$ slip was very difficult. As a result, large incompatibility stresses can build up at α_2/α_2 interfaces causing brittle fracture and reduced strength values. At elevated temperatures, additional $\langle c + a/2 \rangle$ slip can occur, resulting in increased ductility.

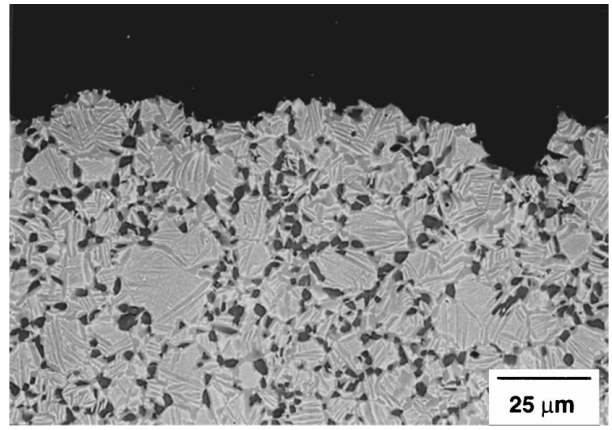

Figure 9 BSE images of the Ti-22Al-26Nb alloy after tensile testing at room temperature.

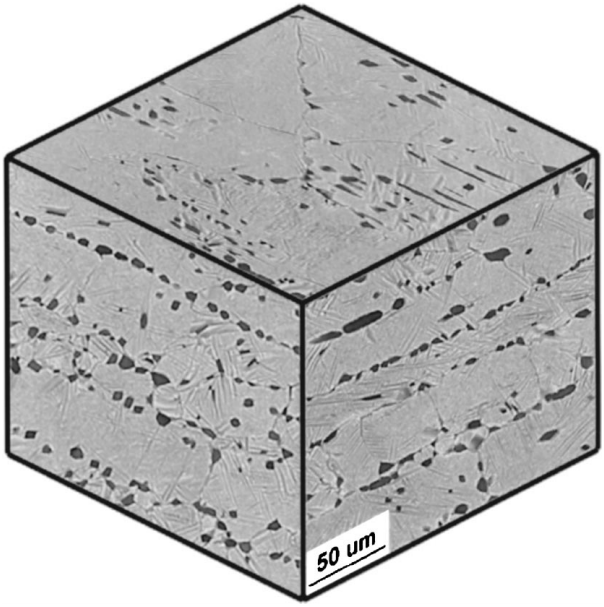

Figure 10 BSE images of the neat matrix microstructure for heat treated foil based Ti-22Al-26Nb.

Additionally, a modest amount of porosity was noted during metallographic preparation and fractography. This porosity, most likely due to incomplete consolidation during the HIP'ing process, has a detrimental effect on all mechanical properties, particularly ductility and fatigue, due to the associated stress concentration.

The Ti-22Al-26Nb foil-based microstructure is shown in Fig. 10. One very noticeable difference compared to the powder-based microstructure is the elongation of the primary α_2 phase. During hot and cold rolling α_2 gets severely microstructurally textured. In addition, crystallographic texturing of the β phase has also been reported [20]. The individual effects of the microstructural and crystallographic texturing on tensile ductility have not been clearly defined to date. However, in neat Ti-22Al-23Nb, unidirectional cold rolling produced significant anisotropy with over 10% room temperature strain-to-failure reported in the direction of cold rolling and only ~2% in a direction perpendicular to the cold rolling direction [21]. Therefore, in composite construction for foil-based systems, one needs to pay particular attention to make certain the fiber direction is coincident with the cold rolling direction of the foil, in order to maximize fiber loading capabilities of the matrix. In addition, no assessment of short transverse (i.e. through-thickness) ductility has been measured for foil-based "O" matrices. It is certainly possible that the elongated α_2 phase which forms a continuous stringer, may result in poor through-thickness strain-to-failure values.

3.2.2. Creep

Fig. 11 displays the elevated temperature creep response as stress versus a Larson-Miller Parameter (LMP) at a creep strain of 0.24% for both the powder and foil-based alloys [16]. A least squares fit to the foil data yields a creep response which is significantly higher than the P/M alloy. Again, the most likely rationale for this is the contiguous nature of the α_2 phase in the P/M system. Banerjee [15] had previously shown that single phase α_2 was inferior to single phase "O" in creep resistance. Therefore, the contiguous nature of the α_2 provides for a preferred low creep resistant fracture path. In addition, previous studies for the Ti-22Al-23Nb foil-based system indicated that like strain-to-failure, microstructural and/or crystallographic texturing had a measurable effect on creep behavior [22]. Therefore, it is possible that texturing of the foil-based alloy may have contributed to the differences between the two systems in creep response.

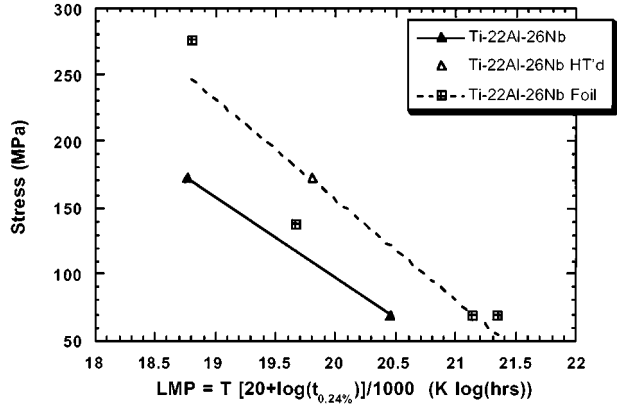

Figure 11 Stress as a function of Larson-Miller parameter (LMP) for 0.24% strain.

3.2.3. Fatigue

Isothermal fatigue tests were conducted at three different temperatures (23°C, 430°C, and 650°C) to generate the stress-life (S-N) curves for the Ti-22Al-26Nb powder-based neat matrix alloy. Some amount of scatter was observed in the results, largely due to material defects that had a considerable influence on fatigue life. The data from obviously flawed samples were discarded based on SEM observations of the fracture surfaces. Fig. 12 depicts the trend in fatigue life as a function of temperature, based on the best-fit S-N curves, at a constant maximum stress ($\sigma_{max} = 550$ MPa) and $R = 0.1$. In addition, neat matrix data from foil-based Ti-22Al-26Nb is shown for comparison [16]. There was a weak trend in the powder-based matrix for an

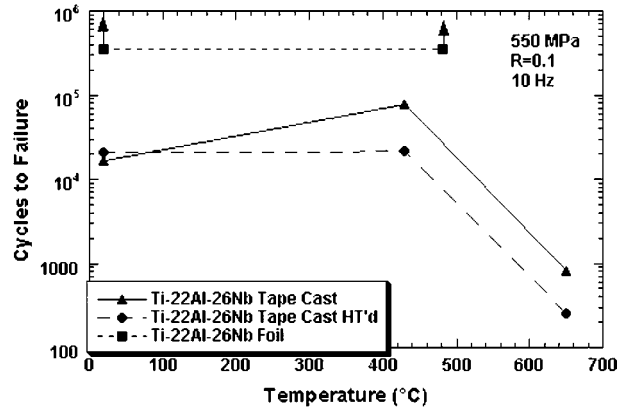

Figure 12 Fatigue as a function of temperature for tape cast, tape cast and heat treated, and foil based Ti-22Al-26Nb.

improvement in fatigue resistance at the intermediate temperature, 430°C, with a more significant reduction at 650°C. The increase in life at intermediate temperatures for the powder alloy may have been the result of an increase in ductility, (>5% at 430°C compared to 1.1% and 2.4% at 23°C and 650°C, respectively). There was, however, no drastic change in the fracture behavior at the intermediate temperature. Fracture typically occurred by cleavage within the α_2 with more tortuous, transgranular fracture observed in the $O + \beta$ regions. The decrease in life at 650°C was likely the result of environmental degradation via interstitial embrittlement. Specimens tested at 650°C contained clear indications of an embrittled surface layer (Fig. 13) that may have aided crack initiation and propagation. The fatigue lives associated with the powder-based matrix was clearly inferior to that observed for the foil-based system. The rationale for this debit was thought to be attributable to internal defects found in the powder-based matrix. Fig. 14 shows a fatigue initiation site associated with internal porosity. This porosity in turn was attributable to incomplete consolidation of the neat matrix during HIP'ing. The porosity acts as an area of increased stress concentration and a site for premature initiation. The end result being reduced fatigue performance.

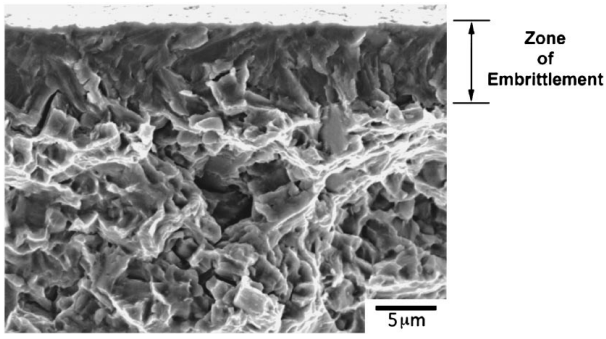

Figure 13 Typical embrittled surface layer.

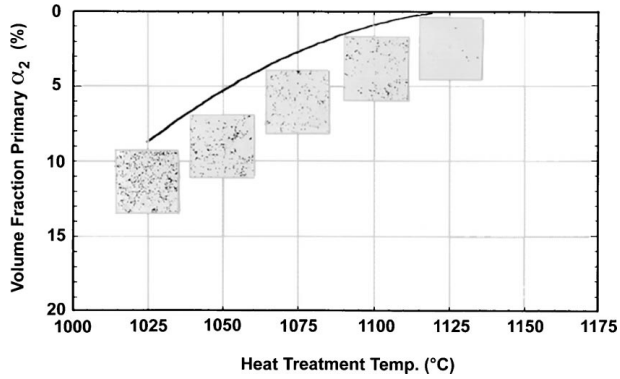

Figure 15 The β_0 solvus approach curve as determined by the disappearing phase technique.

3.3. Heat treated microstructure and mechanical properties

3.3.1. β solvus determination

Fig. 15 contains the β solvus approach curve as determined for the powder-based Ti-22Al-26Nb alloy by the disappearing phase technique. It can be noticed that the β solvus temperature is approximately 1125°C. Table IV contains the β solvus temperature as determined by DTA. As can be seen, transus temperatures ascertained from the heating and cooling data matched rather closely and were in good agreement with the values determined by the disappearing phase technique.

3.3.2. Preliminary heat treatments

Heat treatments were undertaken for the powder alloy in an attempt to dissolve as much of the α_2 phase as

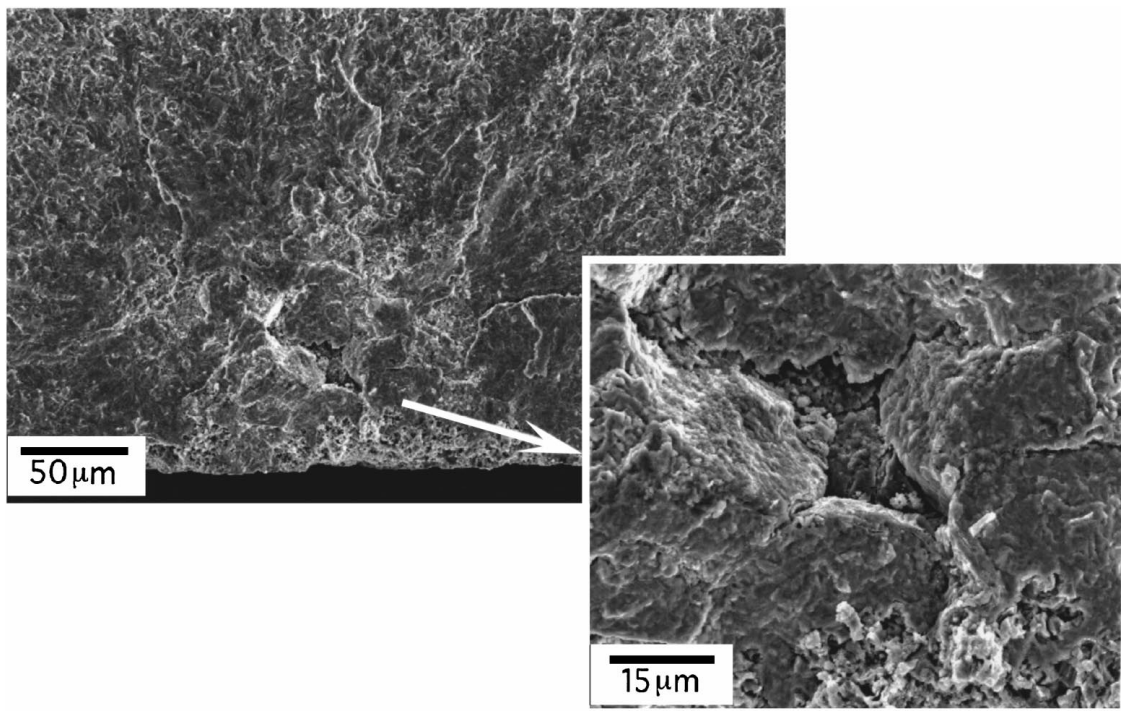

Figure 14 Fatigue initiation at internal porosity.

TABLE IV The β_0 solvus temperatures as determined by DTA and the disappearing phase approach

Alloy	β_0 solvus (°C) DTA (Heating)	β_0 solvus (°C) DTA (Cooling)	β_0 solvus (°C) Disappearing Phase	β_0 solvus (°C) Used in Study
Ti-22Al-26Nb	1121	1118	1125	1125

TABLE V Preliminary heat treatments used to dissolve α_2 phase

Alloy	Heat Treatment
Ti-22Al-26Nb	1100°C/24 hrs cool @ 5°C/m to 815°C/8 hrs/FC
Ti-22Al-26Nb	1150°C/10 mins cool @ 5°C/m to 815°C/8 hrs/FC

TABLE VI Effect of preliminary heat treatment on α_2 content

Alloy	Condition	$V_f\,\alpha_2$ (%)
Ti-22Al-26Nb	As-Consolidated	17.1
	1100°C/24 hrs cool @ 5°C/m to 815°C/8 hrs/FC	12.3
	1150°C/10 mins cool @ 5°C/m to 815°C/8 hrs/FC	10.4

possible, while limiting the growth of the beta grain structure. Thus, heat treatments were conducted for each alloy that incorporated both sub-solvus (β solvus-25°C) and super-solvus (β solvus + 25°C) solutionizing followed by direct cooling (5°C/min) to a constant stabilization aging treatment (815°C/8 hrs). The preliminary heat treatments utilized are shown in Table V. It should be noted the heat treatments were selected to be compatible with (and possibly incorporated into) the consolidation cycle for the manufacture of fiber reinforced O TMCs. As such, the cooling rate was limited to 5°C/min, which corresponds to the maximum rate which can be obtained in the fabrication of an O TMC component incorporating large tooling in a HIP'ing operation [23]. In addition, the cooling rate is also limited during manufacturing in order to prevent component distortion due to mismatch in coefficient of thermal expansion (CTE) between the fiber reinforcement and the "O"-based matrix. The time at solution temperature varied significantly depending upon whether the thermal treatment was sub-solvus or super-solvus. Times for super-solvus solutionizing were kept very short (i.e. $\leq$10 minutes) to minimize prior beta grain growth and dissolution of carbon from the SiC reinforcements.

3.3.3. Microstructure

Fig. 16 contains BSE images for the powder-based alloy after being subjected to the preliminary sub-solvus and super-solvus heat treatments. It can be noticed that the volume fraction of the primary α_2 phase has decreased (10.4–12.3%) as compared to the as-consolidated condition (17.1%) with the super-solvus treatment yielding even lower levels (Table VI). The sub-solvus and super-solvus heat treatments both resulted in significant coarsening of the O + β structure, as well as, some growth of prior beta grain structure. In addition, the super-solvus solutionizing and slow cooling has resulted in the decoration of the prior β boundaries with a continuous network of α_2 and/or "O".

3.3.4. Heat treatment selection

Room temperature tensile properties (Table VII) were determined for the powder alloy after being subjected to the aforementioned preliminary heat treatments. The first criterion used to select those heat treatments for further mechanical property characterization was that of room temperature strain-to-failure. As was previously noted, a minimum room temperature strain-to-failure of ~2.5–3.0% is required in the matrix to overcome tensile residual stresses due to CTE mismatch and to fully load the SiC reinforcement, thereby enabling rule-of-mixtures tensile strengths to be obtained in the composite. It can be noticed that both the sub-solvus and super-solvus heat treatments resulted in improved levels of room temperature ductility for the powder-based neat Ti-22Al-26Nb. In fact, the sub-solvus strain-to-failure (2.8%) now falls within the range of that required to be considered for a composite matrix.

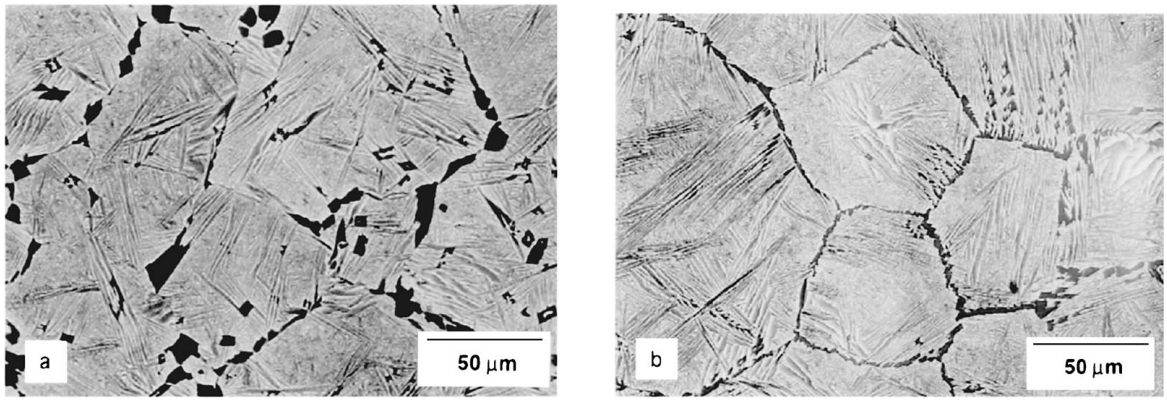

Figure 16 BSE images of neat material after being subjected to the preliminary sub-solvus (a) and super-solvus (b) heat treatments.

TABLE VII Effect of preliminary heat treatment on room temperature tensile properties

Alloy	Condition	UTS (MPa)	YS (MPa)	%El	Mod (GPa)
Ti-22-26	As-Consolidated	921	845	1.1	121
	Sub-Solvus*	881	658	2.8	122
	Super-Solvus	858	601	2.3	121

*Selected for further mechanical properties evaluation.

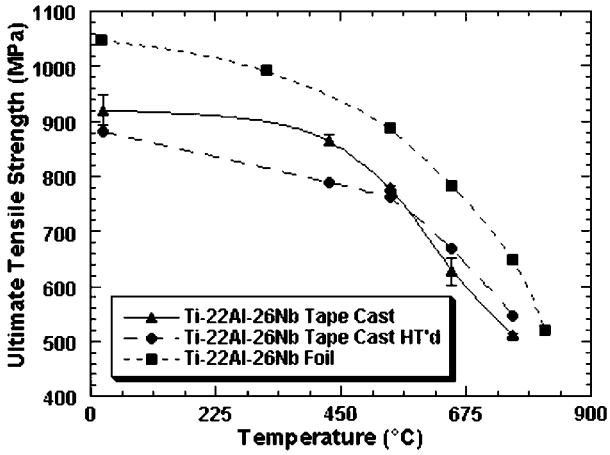

Figure 17 Ultimate tensile strength as a function of temperature for Ti-22Al-26Nb alloy in as-consolidated, consolidated plus heat treated, and foil processed conditions.

Based upon the room temperature strain-to-failure results for the sub-solvus heat treatment, it was selected for further investigation of tensile, fatigue and creep performance.

3.3.5. Heat treated tensile properties

The room temperature strain-to-failure for the heat treated powder-based neat Ti-22Al-26Nb is shown in Fig. 8. The increase in ductility occurred only at room temperature, where the higher strain-to-failure is necessary to fully load a composite. At higher temperatures, the heat treatment produced no increase in ductility. Fig. 17 contains the UTS versus temperature for the powder-based and foil-based Ti-22Al-26Nb alloys. It can be noticed that the sub-solvus heat treatment has resulted in a slight debit in UTS compared to the as-fabricated condition for the powder-based system at temperatures $<540^{\circ}$C. It can been seen, comparing Fig. 5 and Fig. 16a, that the scale of the sub-solvus microstructures (α_2 grain size, O platelet size, and $O + \beta$ colony size) increased dramatically compared to the as-consolidated condition. For the sub-solvus condition, the α_2 grain size increased from $\sim$2–3 μm to $\sim$10 μm, while the number of α_2 grains correspondingly decreased resulting in a reduced volume fraction of primary α_2 (17.1% down to 12.3%). Additionally, this decrease in the number of primary α_2 grains, which had been effectively acting to "pin" the $O + \beta$ colonies, enables additional growth of these colonies during heat treatment ($\sim$10 μm up to $\sim$25–50 μm). The combination of the larger grain and colony sizes were most likely responsible for the reduction in UTS observed at lower temperatures due to Hall-Petch considerations.

It can also be noticed that the foil-based alloy demonstrates a consistent 80–120 MPa increase in UTS compared to the powder-based system. Although the microstructure of the foil-based alloy was not the subject of the present investigation, it appears as though microstructural and/or crystallographic texturing of this alloy during hot and cold rolling to foil, may have contributed to its increased levels of strength.

3.3.6. Heat treated creep properties

The creep performance of the heat treated powder-based neat Ti-22Al-26Nb is shown in Fig. 11 in addition to the as-fabricated powder-based and foil-based Ti-22Al-26Nb alloys in terms of stress versus a Larson-Miller parameter at a creep strain of 0.24%. Although limited data was collected on the sub-solvus heat treated powder-based alloy, it can be noticed that the heat treatment significantly improved the creep resistance compared to the as-fabricated condition. In fact, the creep performance of the heat treated powder alloy is now very similar to that for the foil-based material. This increase in creep resistance is most likely the result of two factors: 1) increased levels of lenticular "O" phase, accompanied by decreased levels of equiaxed primary α_2; and 2) increased grain and colony sizes.

3.3.7. Heat treated fatigue properties

The effect of the heat treatment on the fatigue performance of the powder-based Ti-22Al-26Nb alloy is shown in Fig. 12 and compared to the foil-based Ti-22Al-26Nb system, as cycles to failure versus temperature at a maximum stress of 550 MPa, $R = 0.1$ and a frequency of 10 Hz. There appeared to be a slight debit in fatigue life associated with the sub-solvus heat treatment, when compared to the as-fabricated condition for the powder alloy, particularly at higher temperatures. This decrease may be associated with the increased levels of lenticular "O" phase and decreased levels of equiaxed primary α_2. Previous studies [24] on Ti-22Al-23Nb in monolithic form, indicated that increasing the lenticular "O" phase content at the expense of equiaxed α_2, resulted in a less fatigue initiation resistant microstructure. With the internal defects present in the powder-based matrix (including the aforementioned porosity) providing for higher stress concentration sites, reducing the fatigue initiation resistance of the microstructure may have enabled premature initiation compared to the as-fabricated condition. Therefore, the internal defects associated with the powder-based material results in significantly lower fatigue lives when compared to the foil-based system.

4. Conclusion

The subject study has demonstrated that an orthorhombic-based titanium aluminide alloy, Ti-22Al-26Nb (at%) can be gas atomized into spherical powder form

with good control of both the main alloying constituents and interstitial elements. Upon solidification during the atomizing process, microsegregation of Al occurs in the dendritic boundaries such that they are rich in Al and lean in Nb. Consolidation of tape cast green tapes via HIP'ing into neat (unreinforced) material, results in a three phase microstructure: "O", β and α_2. The phases are present as a lenticular "O" platelets (ordered), in a β matrix (disordered), with a contiguous network of primary α_2 (ordered) being formed in the Al-rich regions as a result of the microsegregation in the starting powder. This contiguous network of primary α_2 with its limited slip characteristics is predominantly responsible for the low room temperature ductility ($\sim$1%) observed in the as-consolidated neat material. This ductility is significantly less than that required for use as a matrix material ($\sim$2.5–3.0%) in the formulation of a SiC fiber reinforced metal matrix composite necessary to overcome the mismatch in fiber and matrix CTE, and to fully load the fiber to its maximum strain capability. Solution heat-treating below the β-solvus and direct aging, results in increases in room temperature ductility (2.8%) into the range requisite for a composite matrix. In addition, the creep performance of the heat treated matrix is improved to levels commensurate with those found in foil-based versions of the Ti-22Al-26Nb alloy due to increases in lenticular "O" phase and decreases in equiaxed α_2. Isothermal fatigue performance of the powder-based alloy, in both the as-consolidated and heat treated conditions, was significantly lower than those found in the foil-based system. This debit is most likely the result of internal defects including porosity due to incomplete consolidation.

Hence, it would appear that a heat treated version of the P/M-based Ti-22Al-26Nb matrix would be viable for composite fabrication in terms of both matrix ductility required to fully load the continuous SiC fiber, and matrix creep resistance. It should be noted however, that carbon dissolution from the SiC fiber coating may occur during heat treatment, which could potentially reduce the matrix ductility below requisite levels. In addition, internal defects present in the P/M-based matrix may act as stress concentration sites and provide for early crack initiation. However, this latter issue may be mitigated to some degree, if a significant portion of the composite's fatigue life were to be spent in crack propagation (i.e. due to fiber bridging). Furthermore, it may be possible to use the P/M-based Ti-22Al-26Nb as a precursor for wire or foil production as a means to eliminate costly ingot reduction practices. In this instance, significant amounts of cold work would be expected to produce increases levels of ductility due to microstructural and/or crystallographic texturing. However, it would be important to assess possible anisotropy in mechanical behavior due to this texturing.

Acknowledgements

The authors gratefully acknowledge the contributions of Mr. Jon Wilson, University of Dayton Research Institute, for mechanical testing performed under contract AF Contract F33615-98-C-5214, Mr. Mark Dodd for heat treatment, and Mr. Eric Fletcher for specimen preparation both of Universal Energy Systems working under AF Contract F33615-96-C-5258 and F33615-97-C-5274, respectively, as well as, valuable technical discussions with Mr. Cecil Rhodes of Rockwell Science Center.

References

1. S. M. RUSS, A. H. ROSENBERGER and D. A. STUBBS, in "Recent Advances in Composite Materials," edited by S. R. White, H. T. Hahn, and W. F. Jones (American Society of Mechanical Engineers, New York, 1995) p. 13.
2. S. M. RUSS, J. M. LARSEN and P. R. SMITH, in "WL-TR-95-4068 Orthorhombic Titanium Matrix Composites," edited by P. R. Smith (WPAFB, OH, 1995) p. 162.
3. D. B. MIRACLE, P. R. SMITH and J. A. GRAVES, *Material Research Society Proc.* **350** (1994) 133.
4. C. G. RHODES, J. A. GRAVES, P. R. SMITH and M. R. JAMES, in "Structural Intermetallics," edited by R. Darolia, J. J. Lewandowski, C. T. Liu, P. L. Martin, D. B. Miracle and M. V. Nathal (The Minerals, Metals, and Materials Society, 1993) p. 45.
5. P. R. SMITH, J. A. GRAVES and C. G. RHODES, *Materials Research Society Proc.* **273** (1992) 43.
6. *Idem.*, *Metallurgical Transactions* **25A** (1994) 1267.
7. R. G. ROWE, C. G. RHODES, C. C. WOJCIK, P. L. MARTIN, M. R. JAMES, A. CHATTERJEE, J. C. CHESNUTT, J. A. GRAVES and W. H. HANUSIAK, "AFRL-ML-WP-TR-1998-4189" (WPAFB, OH, 1998).
8. R. G. ROWE, D. BANERJEE, K. MURALEEDHARAN, M. LARSEN, E. L. HALL, D. G. KONITZER and A. P. WOODFIELD, in "Titanium '92 Science and Technology," edited by F. H. Froes and I. Caplan (The Minerals, Metals, and Materials Society, 1993) p. 1259.
9. C. F. YOLTON and J. P. BECKMAN, *Materials Science and Engineering* **A192/193** (1995) 597.
10. J. F. EDD and J. T. NIEMANN, "Titanium Matrix Composites, WL-TR-92-4035" (WPAFB, OH, 1992) p. 158.
11. P. R. SMITH and W. J. PORTER, *J. Materials Science* **32** (1997) 6215.
12. J. A. GRAVES, Rockwell Science Center, Thousand Oaks, CA, Unpublished Research, 1993.
13. G. A. HARTMAN and S. M. RUSS, in "Metal Matrix Composites: Testing, Analysis, and Failure Modes, ASTM STP 1032," edited by W. S. Johnson (American Society for Testing and Materials, Philadelphia, PA, 1989) p. 43.
14. C. G. RHODES, in AeroMat '98, Tysons Corner, Va., June 1998.
15. D. BANERJEE, A. K. GOGIA, T. K. NANDY, K. MURALEEDHARAN and R. S. MISHRA, in "Structural Intermetallics," edited by R. Darolia, J. J. Lewandowski, C. T. Liu, P. L. Martin, D. B. Miracle and M. V. Nathal (The Minerals, Metals, and Materials Society, 1993) p. 19.
16. N. E. ASHBAUGH, University of Dayton Research Institute, Dayton, OH, Unpublished Research, 1998.
17. R. A. AMATO and D. R. PANK, in "Titanium Matrix Composites, WL-TR-92-4035," edited by P. R. Smith and W. C. Revelos (WPAFB, OH, 1992) p. 80.
18. R. R. CERCHIARA, Ph.D. thesis, Univ. of Pittsburgh, 1996.
19. D. A. KOSS, D. BANERJEE, D. A. LUKASAK and A. K. GOGIA, in "High Temperature Aluminides and Intermetallics," edited by S. H. Whang, C. T. Liu, D. P. Pope and J. O. Stiegler (The Metallurgical Society, Warrendale, PA, 1990) p. 175.
20. A. D. ROLLETT, P. R. SMITH and M. R. JAME, *Material Science and Engineering* **A257**(1) (1998) 77.
21. M. A. FOSTER, P. R. SMITH and D. B. MIRACLE, *Scripta Materialia* **33**(6) (1995) 975.
22. P. R. SMITH, Materials and Manufacturing Directorate, WPAFB, OH., Unpublished Research, 1992.
23. A. CHATTERJEE, Allison Engine Company, Indianapolis, IN, private communication, 1998.
24. S. LUETJERING, PhD. thesis, Univ. of Dayton, 1998.

Received 15 October
and accepted 22 December 1999